Experimental and numerical study of a three-blade horizontal turbine in a wind tunnel

Luis César Delgado-Escobar [1], Valaur Ekbalam Márquez-Baños [2], Román Guadarrama-Pérez [3], Felipe González-Montañez [1], Victor M. Jimenez-Mondragón [1], Javier Valencia-López [4], Alejandra Manuela Vengoechea-Pimienta [1], y Jorge Ramírez-Muñoz [1,*]

[1] Departamento de Energía, DCBI, Universidad Autónoma Metropolitana unidad Azcapotzalco, Azcapotzalco, CDMX, México
[2] Área de Química, Departamento de Preparatoria Agrícola, Universidad Autónoma Chapingo, Texcoco, Estado de México, México
[3] Departamento de Ingeniería Química, TecNM/Instituto Tecnológico Superior de El Mante, Ciudad Mante, Tamaulipas, México
[4] Departamento de Procesos y Tecnología, DCNI, Universidad Autónoma Metropolitana unidad Cuajimalpa, Cuajimalpa, CDMX, México
* Autor de correspondencia: jrm@azc.uam.mx; Tel.: +52 55-53189000, ext. 2195

Received: June 26, 2025 Accepted: October 2, 2025 Published: January 26, 2026
DOI: https://doi.org/10.56845/rebs.v8i1.679

Abstract: Electricity generation from renewable sources is essential for sustainable development and is particularly critical in regions affected by energy poverty. In this context, micro-scale wind turbines offer a viable alternative for electrifying isolated rural communities. This study evaluates, experimentally and numerically, the performance of a three-bladed horizontal-axis wind turbine designed to operate under controlled conditions in a wind tunnel. The turbine was fabricated by 3D printing and tested in the wind tunnel of the Autonomous Metropolitan University–Azcapotzalco, Mexico. Steady-state numerical simulations were performed in ANSYS Fluent using the k-ω SST turbulence model. The computational domain was discretized with polyhedral and hexahedral elements under Multiple Reference Frame (MRF) rotational conditions. A mesh-independence analysis based on the numerical torque was conducted, resulting in an optimal mesh of 2,191,718 elements. The numerical model was subsequently validated against experimental data, showing an average torque deviation of 9.27%. Flow visualization through streamlines and velocity-magnitude contours revealed unwanted vortices in the tail-vane region, which induced flow instability and mechanical vibrations in the current design. These effects should be mitigated in future design improvements. The turbine efficiency curve was obtained from electrical power measurements under different resistive loads, adjusted via a light-bulb resistance board, at a wind-tunnel speed of 18.19 m/s. The maximum efficiency achieved was 24%, corresponding to a generated power of 15.2 W at a rotational turbine speed of 3224 RPM. The results validate the proposed CFD model and provide a solid basis for future design optimization of micro-scale wind power systems for rural applications.

Keywords: wind energy, small-scale wind turbine, CFD simulation, wind tunnel, wind turbine efficiency

Introduction

Access to electrical energy is fundamental to human development, as it enables essential services such as potable water, sanitation, healthcare, education, lighting and transportation (Sánchez-Santillán, 2021). At the domestic level, energy availability directly influences well-being and productivity by enabling cooking, ventilation, lighting, and the use of electronic devices (Espinosa-Dorado & Carrillo Núñez, 2021).

However, despite the growing recognition of the importance of energy access, millions of people worldwide still lack it, primarily due to high costs or insufficient electrical infrastructure (Espinosa-Dorado & Carrillo Núñez, 2021). This condition is known as energy poverty. To address this challenge, in 2015 the Member States of the United Nations (UN) established Sustainable Development Goal (SDG) No. 7, which aims to ensure universal access to affordable, reliable, and modern energy by 2030 (UN, 2015). Although significant progress has been made, reducing the share of the global population without electricity from 13% in 2021 to 9% in 2023, equivalent to 675 million people, there is still much work to be done (UN, 2023).

In Mexico, the National Institute of Statistics and Geography (INEGI) reported that around 1% of the population lacked adequate electricity access in 2020, representing about 1.2 million people living under energy poverty conditions (INEGI, 2020). This situation particularly affects rural and marginalized communities, where grid expansion is often economically unfeasible.

Renewable energy technologies, particularly micro-scale wind energy systems, offer a sustainable alternative for meeting the basic electricity demands of isolated communities. Micro-scale wind turbines, typically generating between 100 and 500 W, provide advantages such as compact size, low cost, and simple installation, making them suitable for rural electrification, community projects, or educational applications (Zemamou, Aggour & Toumi, 2017).

A conventional wind energy system consists of a turbine, an electric generator, a power electric converter, and an energy storage unit (Ramírez, Parra & González, 2012). The turbine converts wind kinetic energy into mechanical energy, which is then transformed into electrical power in the generator (Escobar-Díaz & Barrero-Páez, 2009). Because the generator performance depends on the aerodynamic torque produced by the turbine, optimizing the rotor design is crucial for efficient operation.

For this reason, various researchers have focused on turbine design, evaluating parameters such as the orientation of the rotation axis (horizontal or vertical), the number and spacing of blades, and the torsion angle, among others, to maximize the capture of kinetic energy. According to Betz's law, only about 60% of the wind's kinetic potential can theoretically be converted into usable energy (Betz, 1966). In the market, different turbine types are available, particularly Savonius type turbines, which are vertical-axis devices characterized by their ability to operate independently of wind direction and with relatively low wind speeds. These turbines can capture up to 37% of the wind's potential energy (Zemamou, Aggour & Toumi, 2017).

Although the technologies mentioned have produced excellent results, they also present certain disadvantages, such as visual and noise pollution generated by wind systems (Van der Zwaan & Rabl, 2003). Therefore, there is still a broad field of study aimed at optimizing the design of these energy generation systems. In the development of micro-scale wind turbines, Computational Fluid Dynamics (CFD) has become a key tool to optimize design and improve energy conversion efficiency (Arpino *et al*., 2017; Lanzafame *et al*., 2013). Through CFD, it is possible to analyze airflow behavior around the turbine, evaluate the impact of different design parameters, and predict aerodynamic performance before constructing a physical prototype (Kale *et al*, 2013; Wang & Zhan, 2013).

In this work, the efficiency of a three-blade turbine is analyzed under controlled conditions in a wind tunnel. In addition, a CFD model of the same turbine was developed and validated using experimental data, allowing for future improvements to this design.

Materials and Methods

The turbine radius, measured from the center of rotation to the blade tip, is 11.2 cm. Experimental tests were conducted at a wind speed of 18.2 m/s in the wind tunnel of the Autonomous Metropolitan University–Azcapotzalco, facility designed to generate a controlled and uniform airflow within a confined section. The experimental setup is shown in Figure 1. It should be noted that a wind speed of 18.2 m/s is relatively high for the continuous operation of a micro-scale wind turbine; however, this velocity was intentionally selected to evaluate the structural response and maximum performance of the rotor under high-load conditions, which is essential for defining its safe operational limits.

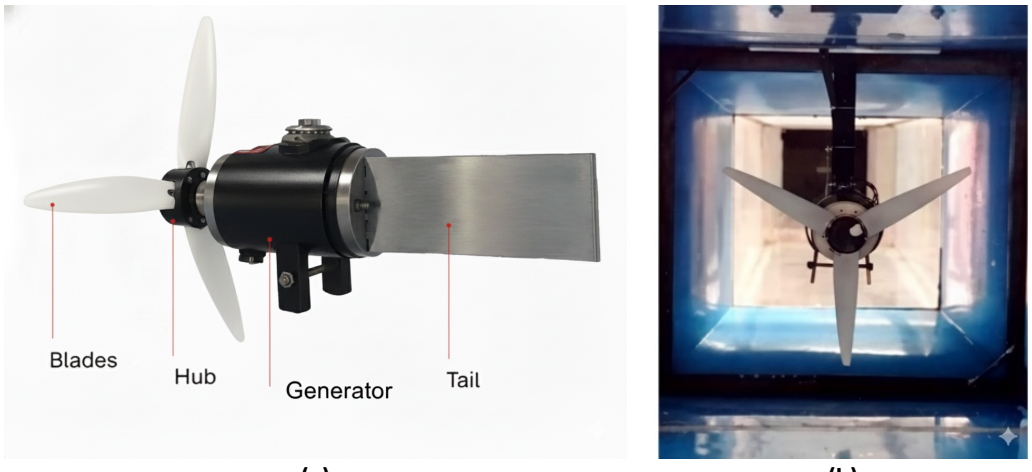

(a) **(b)**

Figure 1. (a) Three-blade wind turbine and (b) turbine mounted in the experimental wind tunnel

The efficiency of the wind turbine under steady wind conditions (18.2 m/s) was evaluated from electrical voltage and current measurements as a function of the applied resistive load. The load bank consisted of sixteen 7.5 W incandescent light bulbs connected in parallel, used as resistive elements to draw electrical power from the generator. The bulbs were mounted on a load board equipped with a digital multimeter for data acquisition, as shown in Figure 2.

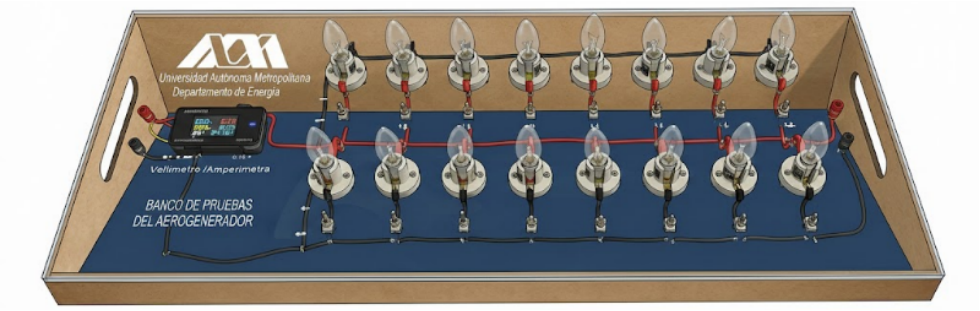

Figure 2. Board of 16 resistive loads (light bulbs) connected in parallel

Using this board, the turbine energy conversion efficiency (η) was calculated as the ratio of the electrical power generated by the DC turbine (P_{elec}) to the wind power (P_v), multiplied by the Betz limit, as expressed in Equation 1.

$$\eta = \frac{P_{elec}}{P_v} = \frac{V \cdot I}{0.593\left(\frac{1}{2}\rho A v^3\right)} \quad \textbf{(1)}$$

where ρ is the air density, A the projected area of the turbine, v the wind velocity, and V and I represent the generated voltage and current, respectively.

To validate the numerical simulations, in situ measurements were performed to quantify the electrical power consumed by the wind turbine installed in the wind tunnel under static conditions (without airflow) and with the rotor operating at the desired speeds. To accomplish this, the wind turbine was driven at specific rotational speeds by regulating the input voltage using a direct current (DC) power supply with an operating range of 0–120 V, as shown in Figure 3. The voltage and current consumed by the turbine were measured using two multimeters: one connected in parallel (for voltage measurement) and the other in series (for current measurement). Power consumption was then calculated as the product of voltage and current. First, the power consumed by the turbine without the rotor (P_{sr}), was recorded, followed by the power consumed with the rotor (P_{cr}), Both power measurements were performed at identical operating speed. The electrical power consumed by the turbine due to the presence of the rotor (P_r), was obtained using the Equation 2.

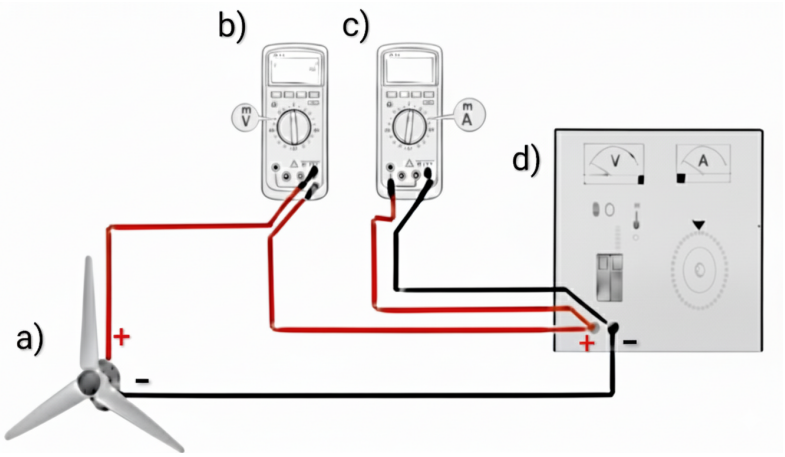

Figure 3. Electrical power measurement system: (a) three-blade turbine (generator DC), (b) multimeter for voltage measurement, (e) multimeter for current measurement, and (f) DC power supply (0–120 V)

$$P_r = P_{cr} - P_{sr} \quad (2)$$

All power values are expressed in watts (W). The experimental torque on the rotor (N·m) derived from electrical power measurements was calculated as follows:

$$\tau_r = \frac{P_r}{2\pi N} \quad (3)$$

where N (s^{-1}) represents the rotor rotational speed.

For the CFD-based simulation, the geometry of the turbine, the motor body, and a section of the wind tunnel were digitally reconstructed. The computational mesh for the wind tunnel–three-blade generator system was generated using ANSYS Fluent Meshing with the Poly-Hexacore method, which produces a polyhedral mesh on the surfaces and hexahedral elements throughout most of the flow domain.

To ensure the numerical reliability of the results, a mesh independence analysis was performed by systematically comparing simulations with different refinement levels until the relative error in the variable of interest (torque) between two consecutive meshes fell below a predefined threshold. The process began with an automatically generated base mesh, followed by successive refinements that approximately doubled the number of elements in each subsequent mesh. The optimal mesh was selected based on the reduction in error between consecutive meshes. Table 1 presents the number of elements used in each case and the corresponding numerical torque values.

Table 1. Mesh independence analysis.

Mesh	Number of Elements	Torque (N·m)
#1	639,139	0.9097
#2	1,080,893	0.6165
#3	2,191,718	0.6500
#4	4,541,751	0.6597

As shown in Table 1, mesh #3, consisting of 2,191,718 elements, provided an appropriate balance between accuracy and computational cost, with an error of only 0.32% compared to mesh #4, even though the latter doubled the number of elements and considerably increased the computational demand. The refined mesh obtained with mesh #3 is shown in Figure 4. Figure 4a illustrates lateral and horizontal cross-sectional views of the elements through the tunnel, while Figure 4b shows the elements on the surface of the rotor blades, generator, and tail.

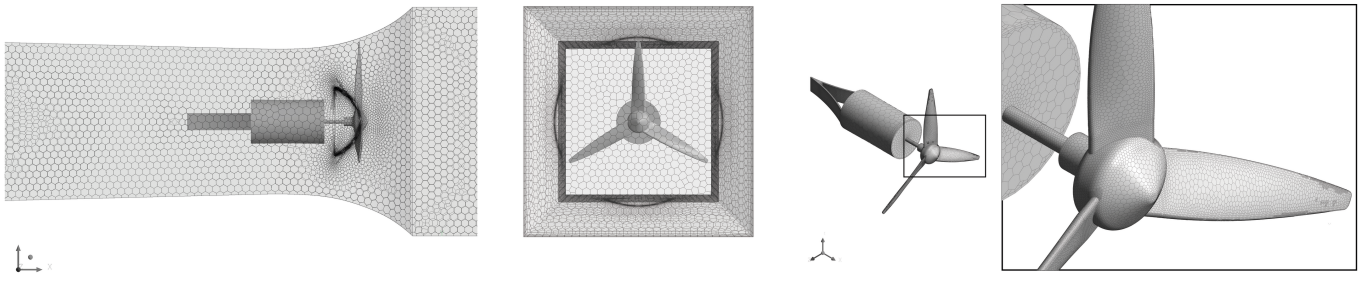

(a) **(b)**

Figure 4. Computational mesh: (a) wind tunnel, (b) three-blade turbine

The turbulent flow within the system was modeled using the k–ω SST turbulence model, which has been widely employed for simulation of wind turbines (Rocha *et al*., 2014; Ji *et al*., 2022, Younoussi & Ettaouil, 2024). The turbine rotation was represented using the Multiple Reference Frame (MRF) approach, based on the experimentally measured rotational speed. As boundary conditions, a no-slip condition was applied to all solid walls, while an inlet velocity of

18.1 m/s matching the experimental conditions was imposed at the front of the wind tunnel. At the outlet, atmospheric pressure was specified. The simulations were performed in ANSYS FLUENT 2025 under steady-state conditions with a convergence criterion of 10^{-5}, using a coupled pressure–velocity scheme. For spatial discretization, the Least Squares Cell-Based method was applied for gradient evaluation, PRESTO! for pressure, and Second-Order Upwind schemes were employed for momentum and turbulence variables.

Results and Discussion

Figure 5 shows the effect of the electrical load (number of light bulbs) on the wind turbine performance in terms of current consumption, voltage, and rotational speed. Regarding current consumption (Figure 5a), a sustained increase is observed up to approximately six light bulbs, reaching a maximum value close to 0.24 A. This is attributed to the decrease in equivalent resistance as the number of parallel loads increases. Beyond this point, the current exhibits a slight decrease and subsequently stabilizes, indicating that the generator can no longer supply more current due to the drastic drop in turbine rotational speed. This behavior is also reflected in Figure 5b, corresponding to voltage, which displays a gradual decrease in the initial load levels, followed by an abrupt drop after six light bulbs, reflecting the loss of rotational speed required to sustain electrical induction. On the other hand, the turbine rotational speed (Figure 5c) presentsa progressive decrease at low loads and a sudden reduction after the same critical point, finally stabilizing below 800 rpm, regardless of the additional load. Overall, the results identify a clear operating threshold around six light bulbs, beyond which the turbine cannot maintain effective energy extraction.

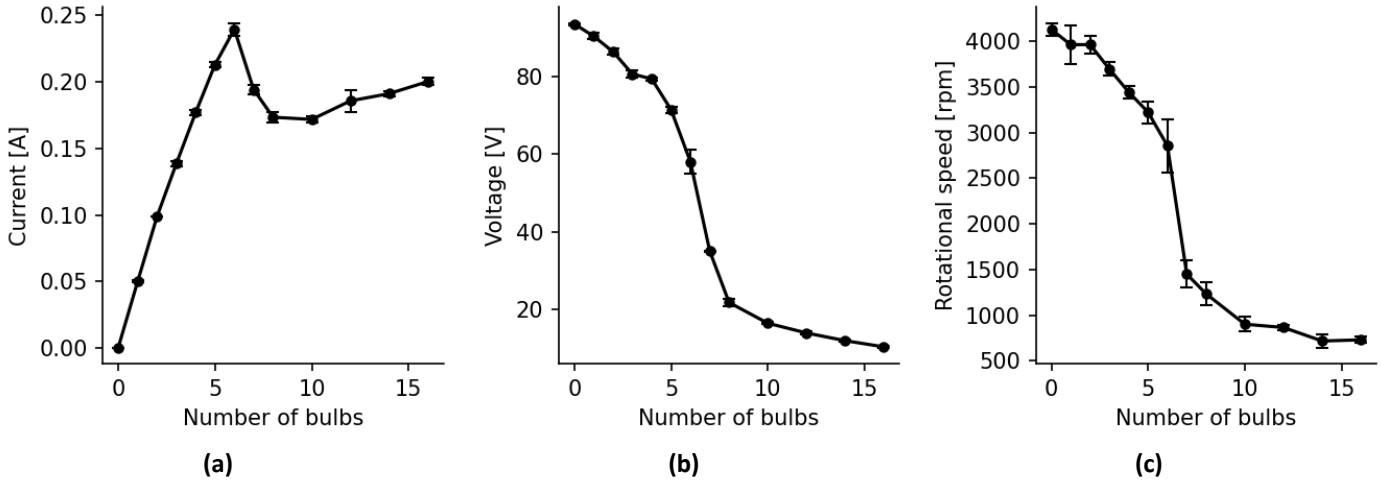

Figure 5. Effect of the electrical load (light bulbs) on (a) current, (b) voltage and (c) turbine rotational speed

The results obtained from Equation 1 are shown in Figure 6, the efficiency increases steadily as the equivalent resistance decreases, reaching a maximum of approximately 0.24 around six lights (Figure 6a), representing the point at which the available aerodynamic torque balances the electrical demand of the load. Beyond this optimal condition, efficiency drops sharply due to the reduction in rotational speed and the consequent decrease in power delivered by the generator. This trend is confirmed in Figure 6b, where efficiency increases almost linearly with current up to approximately 0.20 A, followed by an abrupt drop associated with overload conditions, in which the increased demand does not result in greater energy conversion. The maximum efficiency, corresponding to a generated power of 15.2 W at a wind speed of 18.19 m/s and a rotational speed of 3224 rpm.

Once the maximum efficiency point is exceeded, increasing the load causes a sharp efficiency drop because the rotor speed decreases significantly. When the electrical load increases (i.e., more power is drawn from the generator) at constant wind speed, the resistive torque exerted by the generator on the rotor also increases. If the aerodynamic torque generated by the wind does not increase proportionally, the rotor slows down to balance the extracted energy. Thus, each wind speed has an optimal operating point that maximizes turbine efficiency, known as the optimal tip-speed ratio. Deviating from this point, whether by increasing or decreasing the load, reduces efficiency. A high load slows the rotor speed excessively, while a low load causes the blades to spin too fast, cutting through the air without effectively capturing its energy.

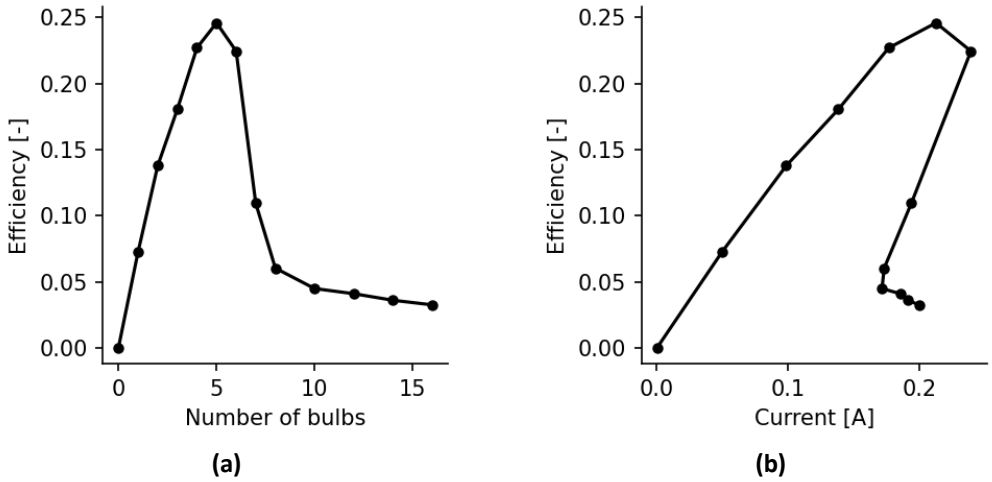

Figure 6. Turbine efficiency, (a) as function of number of resistive loads, and (b) as function of produced current

These results confirm that the wind turbine has a clearly defined operating point to maximize its efficiency, which depends on both the aerodynamic design of the blade and the interaction between the electrical load and the rotor behavior. Identifying this operating point is fundamental for using the system microgeneration applications.

Figure 7 comparesthe experimentally obtained torque values and those obtained through CFD simulation under static conditions. Overall, good agreement is achieved between the two datasets. The relative error between the simulated and experimental values ranged from 4.36% to 12.7%, with an average of 9.27%, confirming the numerical model ability to accurately reproduce the rotor mechanical response. This level of accuracy is consistent with previous studies on small-scale turbines and validates both the use of the k–ω SST turbulence model and the MRF approach for representing the system rotation.

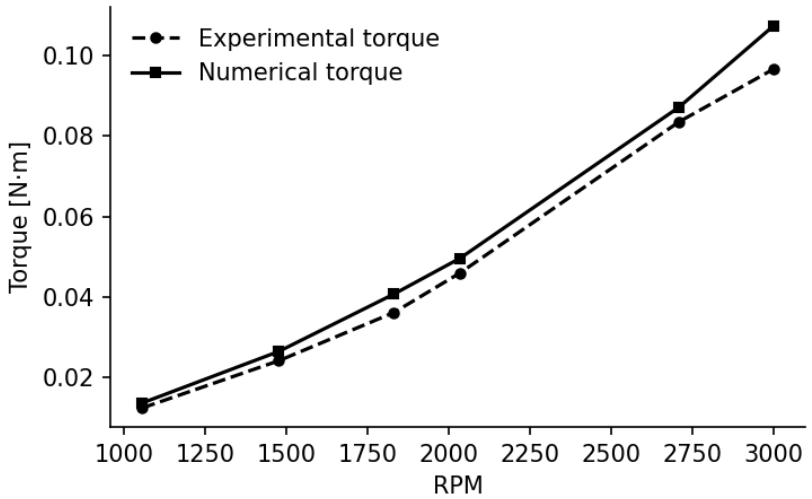

Figure 7. Comparison of simulated and experimental torque values as a function of rotor rotational speed

Figure 8 presents the flow field around and downstream of the turbine, represented by streamlines colored in red and velocity vectors colored with their magnitude show the direction of the flow, close-ups of the wind turbine tail area are also shown. The highest velocity values occur near the rotor blades, especially at the tips. A key observation is the presence of unwanted vortices in the tail region of the wind turbine, whichdisrupts the local velocity field. These structures can induce mechanical instabilities, vibrations, and aerodynamic losses, making them a crucial point to consider in future optimizations of the structural and aerodynamic design.

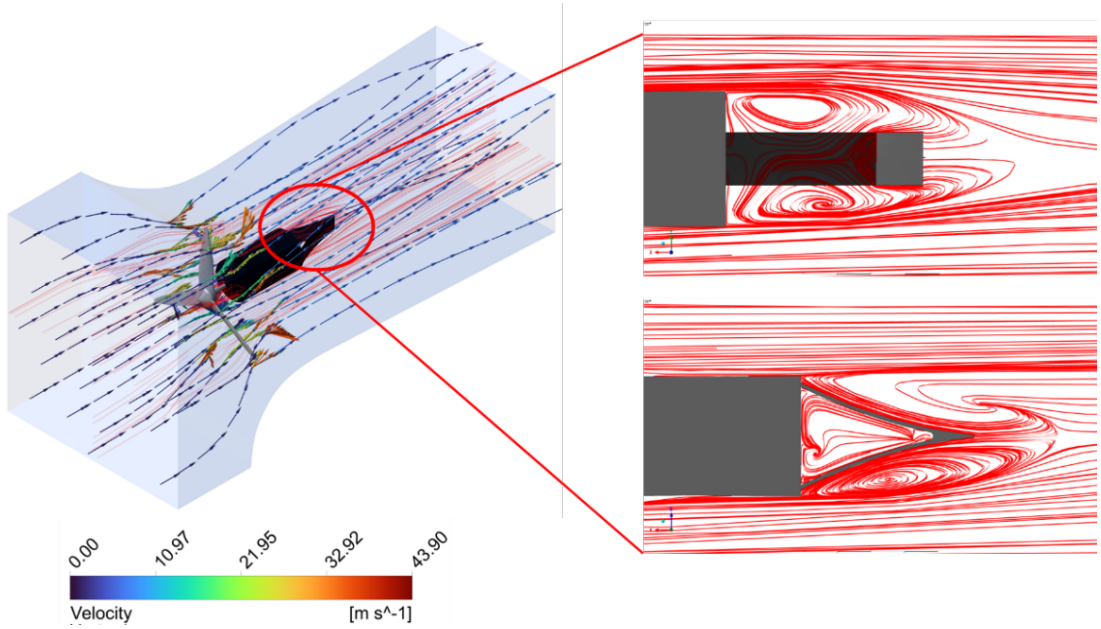

Figure 8. Numerical flow pattern around the wind turbine

On the other hand, the turbulent kinetic energy contours presented in Figure 9 show that the motor body induces a significant region of turbulence, generating a pronounced wake downstream of the wind turbine. This high-energy turbulent zone not only affects the flow pattern around the rotor but can also contribute to load fluctuations and unwanted variations in transmitted torque. These results suggest that it would be necessary to develop a housing with an aerodynamically optimized design for the motor body and tail section in order to minimize turbulence generation, reduce vibrations during operation, and improve the dynamic stability of the system.

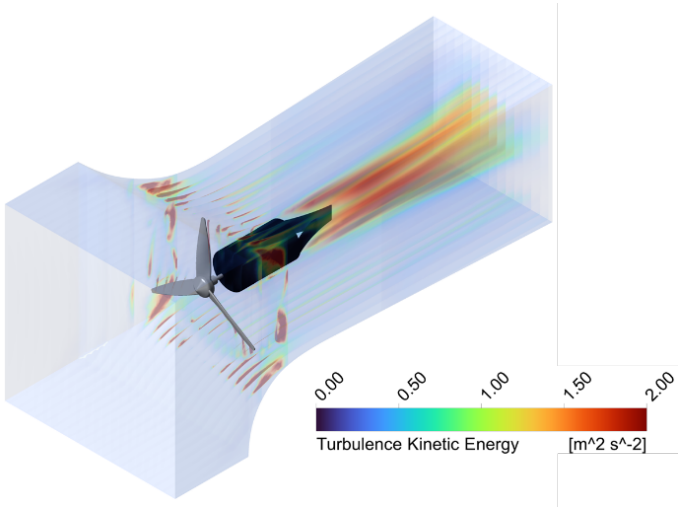

Figure 9. Numerical turbulent kinetic energy contours around the wind turbine

Conclusions

This study evaluated the performance and efficiency of a three-bladed horizontal-axis micro-wind turbine through experimental measurements and numerical simulations. The results demonstrated that the prototype was capable of generation small-scale electrical power efficiently under controlled wind conditions, reaching a maximum output of 15.2 W and a peak efficiency of 24%. Numerical simulations performed with the k-ω SST model and the MRF approach showed strong agreement with the experimental torque values, with a mean deviation of 9.27%, confirming the suitability of CFD as a predictive tool for performance evaluation. The wind tunnel prototype, along with torque and power measurements, provided a solid basis for validating the CFD simulation results.

CFD simulations indicated high turbulence behind the motor casing, suggesting that improvements could reduce wake effects and enhance operational stability. Overall, this study demonstrates that CFD simulations can be effectively used in the development and optimization of low-power wind turbines, contributing to the design of sustainable and accessible renewable energy solutions, especially in rural and off-grid contexts where access to electricity remains limited.

Acknowledgments and Funding: The authors gratefully acknowledge the facilities provided by the thermofluids laboratory of UAM Azcapotzalco and the funding provided by the DPA-UACh to project I-Q-202-25.

Author contributions: L.C.D.-E., A.M.V.-P and J.R.-M: experimental measurements; V.E.M.-B., R. G.-P. and J.V.-L.: design, numerical data collection and analysis and interpretation of data; F.G.-M, V.M.G.-M, A.M.V.-P. and J.R.-M.: conceptualization, supervision and writing.

References

Arpino, F., Cortellessa, G., Dell'Isola, M., Scungio, M., Focanti, V., Profili, M., & Rotondi, M. (2017). CFD simulations of power coefficients for an innovative Darrieus style vertical axis wind turbine with auxiliary straight blades. *Journal of Physics: Conference Series*, *923*(1), 012036. https://doi.org/10.1088/1742-6596/923/1/012036

Betz, A. (1926). *Wind-energie und ihre ausnutzung durch windmühlen* (Vol. 2). Vandenhoeck y Ruprecht.

Escobar-Díaz, A., & Barrero-Páez, L. E. (2009). Modelo matemático de un aerogenerador. *Visión Electrónica*, *3*(2), 48–60. https://doi.org/10.14483/22484728.2835

Espinosa-Dorado, A. L., & Carrillo Núñez, M. P. (2021). Características de la pobreza energética en México: un enfoque desagregado. *Revista Legislativa de Estudios Sociales y de Opinión Pública*, *14*(30), 77–116.

INEGI. (2020). *Información demográfica y social. Censo de Población y Vivienda 2020.*

Ji, B., Zhong, K., Xiong, Q., Qiu, P., Zhang, X., & Wang, L. (2022). CFD simulations of aerodynamic characteristics for the three-blade NREL Phase VI wind turbine model. *Energy*, *249*, 123670. https://doi.org/10.1016/j.energy.2022.123670

Kale, S. A., Gunjal, Y. R., Jadhav, S. P., & Tanksale, A. N. (2013). CFD analysis for optimization of diffuser for a micro wind turbine. *International Conference on Energy Efficient Technologies for Sustainability*, Nagercoil, India, 257–260. https://doi.org/10.1109/ICEETS.2013.6533392

Lanzafame, R., Mauro, S., & Messina, M. (2013). Wind turbine CFD modeling using a correlation-based transitional model. *Renewable Energy*, *52*, 31–39. https://doi.org/10.1016/j.renene.2012.10.007

ONU. (2015b). *Objetivo 7: Garantizar el acceso a una energía asequible, segura, sostenible y moderna*. Recuperado el 16/12/2024 de https://www.un.org/sustainabledevelopment/es/energy/

ONU. (2023). *Informe de los Objetivos de Desarrollo Sostenible. Edición especial* (pp. 26–27).

Ramírez, R. G., Parra, M. S., & González, R. H. (2012). Investigación, desarrollo e innovación tecnológica de sistema del control de aerogeneradores. *Boletín IIE*, abril–junio de 2012.

Rocha, P. C., Rocha, H. B., Carneiro, F. M., Da Silva, M. V., & Bueno, A. V. (2014). k–ω SST (shear stress transport) turbulence model calibration: A case study on a small scale horizontal axis wind turbine. *Energy*, *65*, 412–418. https://doi.org/10.1016/j.energy.2013.11.050

Sánchez-Santillán, O. (2021). *Análisis de la pobreza energética y su impacto en el desarrollo sustentable de México*. Universidad Nacional Autónoma de México, México.

Van der Zwaan, B., & Rabl, A. (2003). Prospects for PV: A learning curve analysis. *Solar Energy*, *74*(1), 19–31.

Wang, Y.-F., & Zhan, M.-S. (2013). 3-dimensional CFD simulation and analysis on performance of a micro-wind turbine resembling lotus in shape. *Energy and Buildings*, *65*, 66–74. https://doi.org/10.1016/j.enbuild.2013.05.045

Younoussi, S., & Ettaouil, A. (2024). Calibration method of the k-ω SST turbulence model for wind turbine performance prediction near stall condition. *Heliyon*, *10*(1). https://doi.org/10.1016/j.heliyon.2024.e24048

Zemamou, M., Aggour, M., & Toumi, A. (2017). Review of Savonius wind turbine design and performance. *Energy Procedia*, *141*, 383–388. https://doi.org/10.1016/j.egypro.2017.11.047